RSC Advances

PAPER

View Article Online
View Journal | View Issue

Check for updates

Cite this: *RSC Adv.*, 2023, **13**, 20271

Study on the effect of fluorinated solvent electrolyte on the active material and cycle performance of a commercial 21700-type battery

Wenbin Liu, Xinyu Li, Yingcai Zhao, Lan Wu and Shu Hong*

Different electrolyte schemes were studied on the traditional commercial 21700-type battery. The effect of different fluorinated electrolytes on the cycle performance of the battery was systematically investigated. When methyl (2,2,2-trifluoroetyl) carbonate (FEMC) was introduced, due to the low conductivity of FEMC, the polarization and internal resistance of the battery increased, which leads to the increase of constant voltage charging time, leading to the cracking of the cathode material and reduction of the cycle performance. When ethyl difluoroacetate (DFEA) was introduced, the poor chemical stability caused by its low molecular energy level led to the decomposition of the electrolyte. Thus, affecting the cycle performance of the battery. However, the introduction of fluorinated solvents can form a protective film on the surface of the cathode, which can effectively inhibit the dissolution of metal elements. The fast-charging cycle of commercial batteries is generally set at 10–80% SOC, which can effectively reduce the H2 to H3 phase transformation process, and the temperature rise caused by fast-charging can also reduce the effect of electrolytic conductivity, so that the protective effect of the fluorinated solvent on the cathode material is dominant. Therefore, the fast-charging cycle performance is improved.

Received 6th April 2023
Accepted 14th June 2023

DOI: 10.1039/d3ra02278a

rsc.li/rsc-advances

Open Access Article. Published on 06 July 2023. Downloaded on 1/19/2026 4:26:41 PM.
This article is licensed under a Creative Commons Attribution-NonCommercial 3.0 Unported Licence.

1 Introduction

Due to the remarkable power and energy density of the lithium battery, it has been applied in a lot of fields, such as digital products, electric vehicles (EVs) and energy storage.[1–7] For lithium batteries used in electric vehicles, their energy and power density requirements are higher, and their cycle life is also facing challenges. The increase of internal resistance and the accelerated decay of the battery at the end of the cycle are considered to be the main factors affecting the cycle life.[8–10] Understanding the relevant degradation mechanisms in batteries is of great importance to optimize the battery lifetime.[11–13] Several aspects have been extensively studied to explore the degradation mechanisms, such as the cathode material,[14–16] anode material,[17] electrolyte,[18–20] septum[21] and so on. Among them, the cathode material and electrolyte attract most attention.

The cathode material is a key factor affecting the cycle life of the battery, especially the nickel-rich ternary material. Ternary materials generally undergo multiple phase transitions during the charging and discharging process of batteries. At the initial stage of lithium removal, the material changes from an initial hexagonal (H1) structure to a monoclinic structure (M), this process will cause the contraction of the *a*-axis in the crystal cell. With the deepening of the degree of lithium removal, the crystal structure of the material gradually changes from monoclinic to hexagonal (H2), which will lead to the increase of the *c*-axis. At the later stage of lithium removal, the hexagonal structure will change into another hexagonal (H3) phase, leading to a sharp contraction of the *c*-axis. The repeated volume changes in the process of charging and discharging process will lead to cracks in the material particles, especially for the secondary particle structure formed by the accumulation of single crystal particles, which usually leads to large area cracks of the ternary material.[22–25] Moreover, the surface of cracked particles may form a layer of NiO-like rock salt phase, which is usually considered as insulator.[26] This transformation of cathode material's structure is considered to be the key factor affecting the cycle life. S. Watanabe *et al.*[27] studied the effect of different discharge depths on particle crack of cathode materials. The cycle performance was performed at 25 °C and 60 °C for the Li$[Ni_{0.76}Co_{0.14}Al_{0.10}]O_2$ cathode/graphite cell. They found that when the discharge depth is low, the contraction and expansion of the material is relatively small, and the degree of particle crack is low. With the increase of the discharge depth, the contraction and expansion of the material gradually increases, resulting in the same trend of particle crack. The effect of temperature is mainly reflected in the case of high discharge depth. When the discharge depth is low (10–70%), the effect of temperature was almost ignored. Y. K. Sun *et al.*[28] reported a new nickel-rich material (Li$[Ni_{0.865}Co_{0.120}Al_{0.015}]O_2$). By

Tianjin Lishen Battery Joint-Stock Co., Ltd, Tianjin 300000, China. E-mail: hong_shu@lishen.com.cn

© 2023 The Author(s). Published by the Royal Society of Chemistry

Open Access Article. Published on 06 July 2023. Downloaded on 1/19/2026 4:26:41 PM.
This article is licensed under a Creative Commons Attribution-NonCommercial 3.0 Unported Licence.

adjusting the gradient distribution of Ni, the design of Ni-rich area at the core and Co-rich layer at the outside was realized. The Ni in the core can improve the capacity of the material, while the Co-rich layer on the surface can increase its stability. Thanks to this unique structural design, the obtained materials showed improved capacity retention and better thermal stability.

Electrolyte also has obvious effect on the cycle life of battery. On the one hand, the conductivity of the electrolyte can affect the polarization and internal resistance of the battery, which may lead to the change of the battery temperature; on the other hand, the electrolyte can obviously promote the formation and stability of solid electrolyte interphase (SEI) film, the decomposition or repeated growth of SEI film may cause the loss of active lithium, which is considered as an important reason for the battery capacity degradation.[29] Z. Zhang *et al.*[30] reported a novel fluorinated electrolyte formulation of fluoroethylene carbonate (FEC)/bis(2,2,2-trifluoroethyl) carbonate (HFDEC) plus lithium difluoro(oxalato) borate (LiDFOB). They evaluated its performance in a conventional lithium battery system with the $LiNi_{0.5}Mn_{0.3}Co_{0.2}O_2$ (NMC532) cathode coupled with the graphite anode. They confirmed that the enhanced oxidation stability, high ionic conductivity and electrode wettability of the fluorinated electrolyte can significantly improve the cycle life and effectively reduce the internal resistance of the battery. Moreover, the fluorinated electrolyte formulation is more conducive to the formation of SEI film on the surface of graphite. Y.-M. Lee *et al.*[31] provided a fluorinated electrolyte additive of 5 wt% methyl (2,2,2-trifluoroethyl) carbonate (FEMC) of fluorinated linear carbonate in the lithium battery system with the $LiNi_{0.5}Mn_{0.3}Co_{0.2}O_2$ (NMC532) cathode. They insist that the FEMC plays a key role in the formation of a stable SEI film and effective passivation of cathode surface, which can improve the cycling performance, discharge capacities and capacity retention. J. R. Dahn *et al.*[32] reported a fluorinated electrolyte formulation of 1 M $LiPF_6$/fluoroethylene carbonate: bis (2,2,2-trifluoroethyl) carbonate (1 : 1 w : w) in a lithium battery system with the $LiNi_{0.4}Mn_{0.4}Co_{0.2}O_2$ (NMC442) cathode coupled with the graphite anode. They found that the fluorinated electrolytes used alone or in combination with other additives showed significant improvement in coulombic efficiency and charge endpoint capacity slippage during the cycle, voltage drop during storage, as well as improving the capacity retention.

Although many studies have been carried out on the effect of cathode materials and electrolyte on battery cycle life, their studies have focused on the individual effects of research objectives. The reduction of battery cycle life is not only the influence of a single factor, but also the synthesis of a series of complex processes. The change of the electrolyte will also have a great effect on the active material. Therefore, it is necessary to comprehensively analyze the effect of electrolyte and cathode materials on the cycle life of battery. Herein, we report effect of the fluorinated electrolyte on battery performance. By adding FEMC and DFEA into the base electrolyte, the effect of fluorinated solvents on the crack of cathode materials and the loss of active lithium was studied. Due to the low conductivity and thermal stability of the fluorinated electrolyte schemes, the conventional cycle of the battery becomes worse, and the crack of the cathode material was aggravated. On the contrary, fluorinated solvents can form a protective cathode electrolyte interface (CEI) film on the surface of the cathode material, which can effectively inhibit the dissolution of metal elements in the active material. Due to the large temperature rise and small charging range during the fast-charging process of the battery, the effect of the electrolyte conductivity is significantly reduced, and the protection of the electrode is dominant. Therefore, the fast-charging ability was improved.

2 Experiments

2.1 Preparation of 21700 batteries

21700 batteries are assembled using a commercial cylindrical battery production process. The cathode material consists of $Li[Ni_{0.88}Co_{0.1}Al_{0.02}]O_2$, acetylene black, and polyvinylidene difluoride (PVDF), with a corresponding ratio of 97 : 2 : 1. The anode material is composed of graphite, silicon, acetylene black, and polymerized styrene butadiene rubber (SBR), with a corresponding ratio of 88 : 8 : 2 : 2. The cathode material, anode material and electrolyte are purchased from commercial electrolyte companies.

2.2 Cycle tests of 21700-type commercial battery

The capacity of 21700-type battery for test is 4.4 A h. The cathode material is $Li[Ni_{0.88}Co_{0.1}Al_{0.02}]O_2$, the anode materials are mainly graphite and silicon. The base electrolyte was a mixture of ethylene carbonate (EC), ethyl methyl carbonate (EMC) and dimethyl carbonate (DMC) containing lithium hexafluorophosphate ($LiPF_6$). The battery using the base electrolyte is marked as BASE-Elect. For comparison, methyl (2,2,2-trifluoroetyl) carbonate (FEMC) and ethyl difluoroacetate (DFEA) were serve as fluorinated solvent and added to the base electrolyte. Batteries with electrolyte fluorinated solvent of FEMC and DFEA are marked as FEMC-Elect and DFEA-Elect respectively. The specifications of tested batteries are shown in Table 1.

2.3 Materials characterization

Powder X-ray Diffraction (XRD, Rigaku-D/max-A) was used to examine the crystalline phase of the cathode materials. The morphology and element content of cathode material were

Table 1 Specifications of the 21700-type lithium battery

Battery type	21700
Cathode material	Ternary material, NCA
Anode material	Graphite and silicon
Electrolyte	Solution of lithium hexafluorophosphate ($LiPF_6$)
Cutoff voltage	2.5–4.2 V
Nominal capacity	4.2 A h
Charging current	4.2 A
Fast-charging current	14.7 A

© 2023 The Author(s). Published by the Royal Society of Chemistry

Open Access Article. Published on 06 July 2023. Downloaded on 1/19/2026 4:26:41 PM.
This article is licensed under a Creative Commons Attribution-NonCommercial 3.0 Unported Licence.

examined by Field-Emission Scanning Electron Microscopy with Energy Dispersive Spectrometer (FESEM with EDS, Carl Zeiss Microscopy Ultra Plus). The average elemental composition analysis of the anode material was tested by an Inductively Coupled Plasma Emission Spectrometry Analyzer (ICP, PerkinElmer Optima8300, USA). The cyclic performance was tested by Arbin battery testing system.

The conductivity of different electrolytes was measured using a conductivity tester (METTLER TOLEDO). The molecular energy levels of different electrolytes were obtained through DFT calculations by Gaussian. The Brunauer–Emmett–Teller (BET) surface areas of the obtained samples were calculated by recording N2 adsorption–desorption isotherms.

3 Results and discussion

3.1 Capacity degradation analysis

Fig. 1a shows the conductivity of the three electrolyte schemes at 25 °C and 45 °C. What can be seen from the figure is that the BASE-Elect exhibited highest conductivity, while the FEMC-Elect showed the lowest conductivity at 25 °C. However, at the temperature of 45 °C, the conductivities of all electrolytes were almost the same, indicating that the effect of electrolyte's conductivity can be ignored at higher temperatures. Fig. 1b shows the molecular energy level of different electrolytes. The DFEA-Elect exhibits a minimum molecular energy level, which indicates that the ability of antioxidant restoration is the weakest, thereby, its chemical stability is relatively poor, which may have a certain effect on the cycle stability of the battery.

In order to verify the stability of the electrolyte, Linear Sweep Voltammetry (LSV) tests were carried out on electrolytes of different schemes. Fig. 2 shows the LSV curves of all electrolyte schemes, it can be seen that there is almost no redox current observed of BASE-Elect, indicating that the electrolyte has good antioxidant reduction ability. An obvious redox current can be observed on the FEMC-Elect scheme, indicating that its antioxidant reduction ability is relative poor. The same change can be observed in DFEA-Elect scheme, where the redox current became more obvious, indicating the worst antioxidant reduction ability than other schemes.

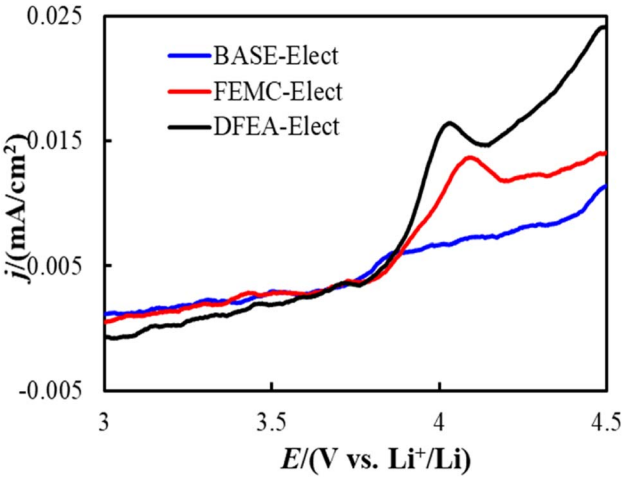

Fig. 2 CV curves of different electrolyte schemes.

Fig. 3a shows the capacity retention rate of three electrolyte schemes at room temperature, the voltage range is 2.5–4.2 V and the charge/discharge current is set to 4.4 A. It can be seen from the figure that the capacity retention rate of all batteries is basically maintained at about 70% at 1000 cycles, which indicates that all schemes have acceptable stability. However, by comparing all the schemes, the BASE-Elect shows the best cycle performance, its capacity retention rate is about 83%, which is relative higher than other schemes. The FEMC-Elect exhibited the lowest capacity retention rate (about 75%), and the

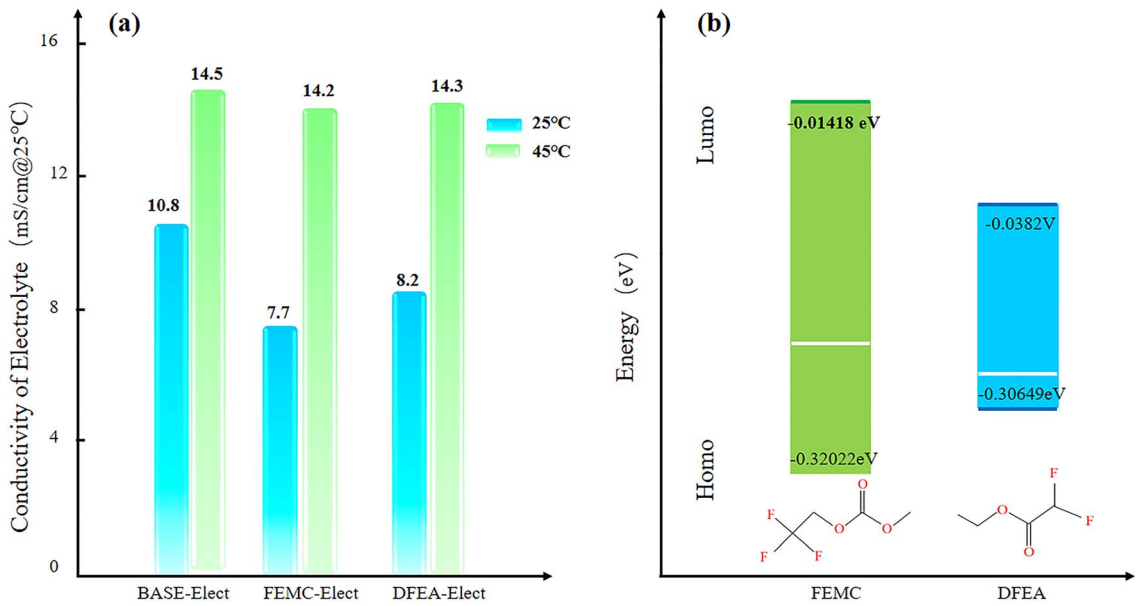

Fig. 1 (a) The conductivity of three electrolyte schemes; (b) the molecular energy level of different electrolytes.

Open Access Article. Published on 06 July 2023. Downloaded on 1/19/2026 4:26:41 PM.
This article is licensed under a Creative Commons Attribution-NonCommercial 3.0 Unported Licence.

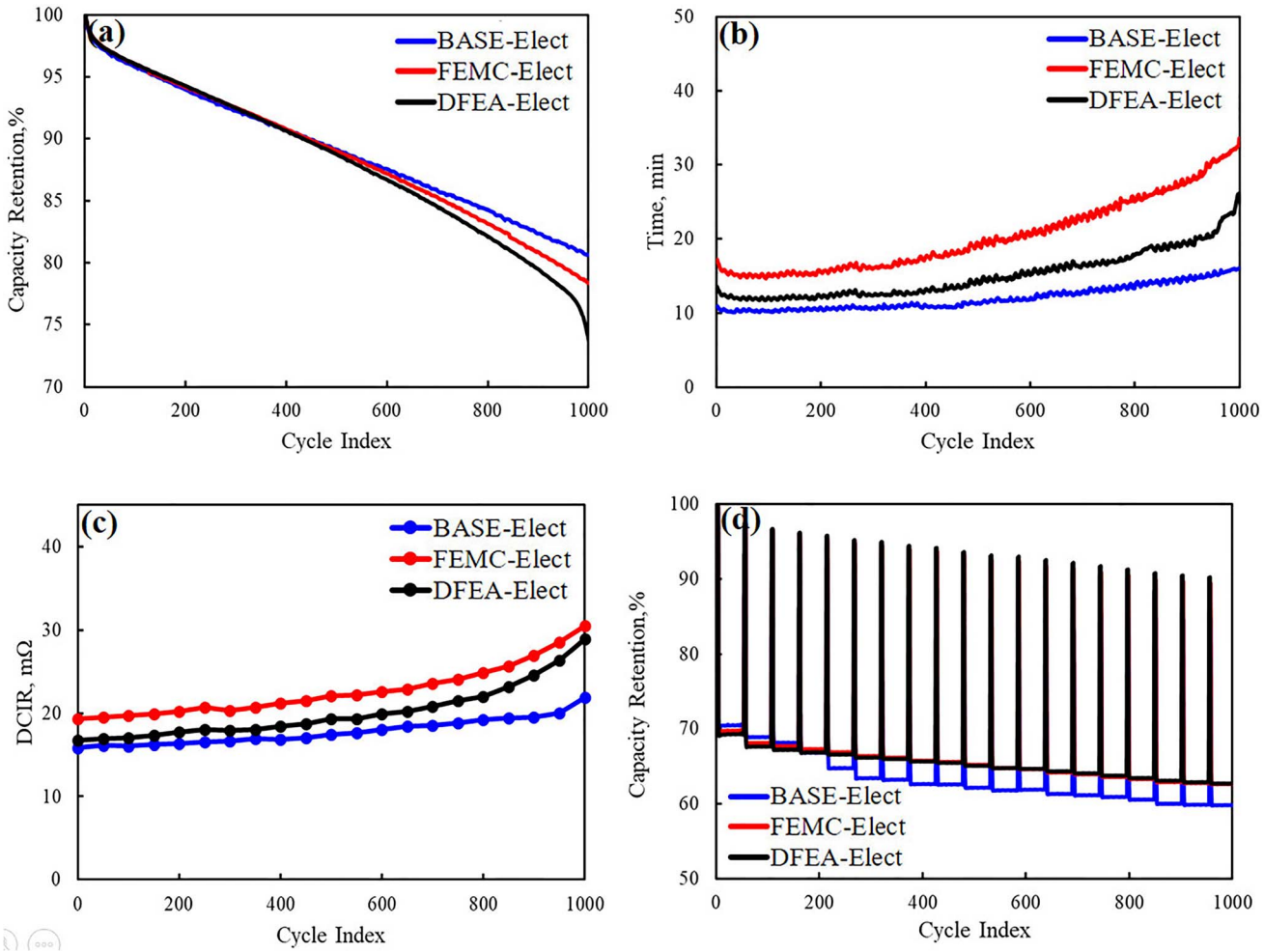

Fig. 3 (a) The capacity retention rate of three electrolyte schemes; (b) the constant voltage charging time of different electrolytes; (c) the growth of the direct current internal resistance (DCIR) of the battery during cycles of three electrolyte schemes; (d) the fast-charging cycle of the different electrolyte schemes.

acceleration attenuation of cycle occurred at the end of the cycle. The occurrence of this phenomenon may be attributed to the lowest molecular level of DFEA, which leads to the worst chemical stability in whole cycles. What's more, some side reactions may occur on the surface of the electrode. Thus, the capacity attenuation of this battery is relatively fast. The capacity retention rate of the FEMC-Elect has also showed a trend of decrease, which may be related to its lower conductivity. The lower conductivity can increase the polarization of the battery, resulting in the increase in the proportion of time for constant voltage charging during the charging process. The increase in charging time under high voltage may lead to the poor use environment of the active material of the battery, especially the cathode material, which may aggravate the crack of the cathode material. Thus, the cycle performance decreased. Fig. 3b shows the constant voltage charging time of the three electrolyte schemes respectively. It can be found that after adding fluorinated solvents, the constant voltage charging time has increased significantly, which is consistent with our previous analysis. The constant voltage charging time of the DFEA-Elect has a significant growth after the 800 cycles, which may be attributed to the poor stability of DFEA. Some side reactions may continuously occur on the surface of the electrode during whole cycles, which accelerates the consumption of the electrolyte. The consumption of the electrolyte led to the rapid decline in the conductivity of the electrolyte, which caused the cycle performance of the battery accelerate attenuation. On the one hand, the consumption of electrolyte will further lead to a rapid decrease in the conductivity of the electrolyte, leading to an increase in polarization; on the other hand, the increase in polarization will increase the temperature of the battery, which may further promote the side reactions of electrolyte. Thus, the cycle performance of the battery is reduced. The same phenomenon can also be observed in the battery of the FEMC-Elect, which means that the cycle performance of this scheme had also deteriorated significantly. Fig. 3c shows the growth of the direct current internal resistance (DCIR) of the battery during cycles. It can be found that since the decrease in electrolytic conductivity caused by the addition of fluorinated solvents, the DCIR of the battery had increased. The growth of the DCIR of the battery is the same as the changes in the constant voltage charging time, which indicates that the

© 2023 The Author(s). Published by the Royal Society of Chemistry

Open Access Article. Published on 06 July 2023. Downloaded on 1/19/2026 4:26:41 PM.
This article is licensed under a Creative Commons Attribution-NonCommercial 3.0 Unported Licence.

reduction of electrolytic conductivity caused by adding fluorinated solvent will increase the internal resistance of the battery, leading to an increase in the internal resistance of the battery. Fig. 3d shows the fast-charging cycle of the different electrolyte schemes, it can be seen from this figure that the fast-charging performance of the battery with fluorinated solvent electrolyte had been significantly improved. This may be due to the large charging current (14.7 A) used for fast-charging, which can lead to the higher temperature rise of the battery. The higher temperature can inhibit the effect of electrolytic conductivity. Moreover, according to the previous report,[19] fluorinated solvent can form the protective CEI film on the cathode, which can protect the cathode material from the corrosion of the electrolyte. Therefore, its fast-charging performance has been improved.

In order to evaluate the proportion of capacity loss caused by the battery polarization, the fresh battery and cycled batteries were performed at the low charge/discharge current (1.4 A and 0.21 A). The results are shown in Fig. 4. It can be seen from the figure that compared with fresh battery, the capacity of cycled batteries under the current of 1.46 A have significantly reduced, however, when the charge/discharge current was set to 0.22 A, some capacity has been restored. It is generally believed that the capacity that can be recovered at a low charge/discharge current is mainly caused by the polarization of the battery, it is also called reversible capacity loss. The difference in capacity at the same charge/discharge current is considered as irreversible capacity loss, that mainly caused by irreversible damage of active materials. For the BASE-Elect, its reversible capacity loss and irreversible capacity loss are relatively small. For the DFEA-Elect, its reversible loss capacity is the highest, but its irreversible capacity loss is lower than the FEMC-Elect, which indicates that the active material of the FEMC-Elect has the greatest damage.

In order to find the reasons for the attenuation of the battery capacity, Fig. 5 show the capacity incremental curves (IC, DQ/DV) of fresh battery and cycled batteries. It can be seen from the figure that all batteries have obvious peaks around 3.6 V, 3.8 V and 4.1 V, corresponding to the phase transformation process of H1 to M, M to H2 and H2 to H3 of ternary cathode material.[33] By comparing with fresh battery, it can be found that the phase transformation peaks of H1 to M and H2 to H3 of cycled batteries were relatively weak, and the peak area was significantly reduced, which indicates that the phase transformation process became weakened, and the capacity had also decayed. However, the phase transformation process of M to H2 had become more obvious, which indicates that the M to H2 phase transformation process of the cycled batteries contributed more capacity. For ternary cathode material, the phase transformation of H1 to M causes the contraction of a-axis in the lattice, and the M to H2 phase transformation process will lead to an increase of a-axis, the H2 to H3 phase transformation process will cause the c-axis contraction. The repeated changes in the lattice parameter in the charging process can cause the stress concentration inside the material, which makes the particles crack. Especially in the H2 to H3 phase transformation

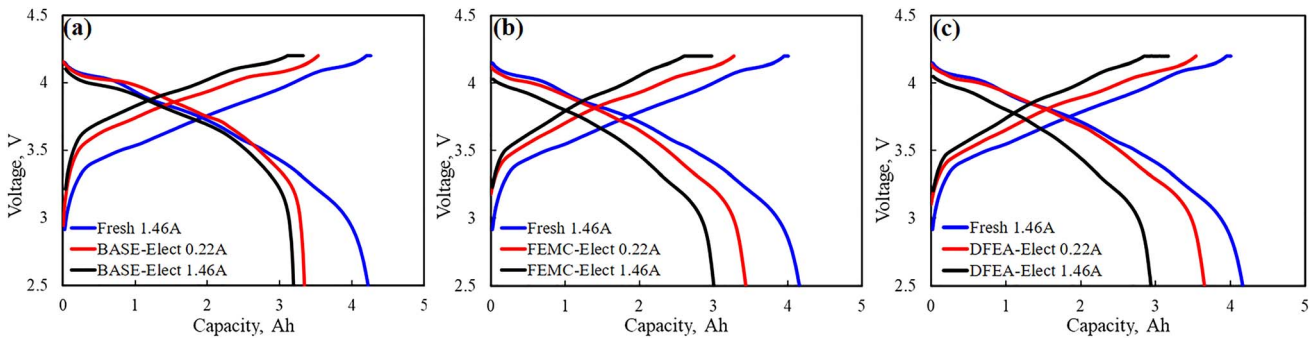

Fig. 4 Charge and discharge curves of batteries with different electrolyte schemes and fresh battery under different current. (a) BASE-Elect; (b) FEMC-Elect; (c) DFEA-Elect.

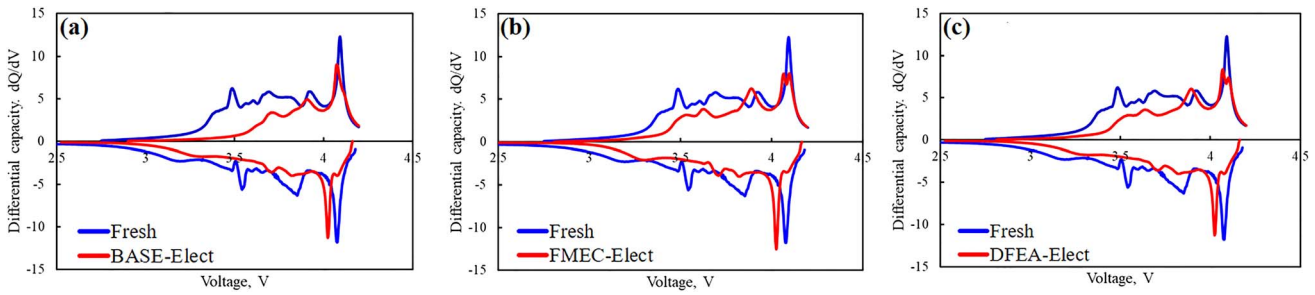

Fig. 5 The capacity incremental curves (IC, DQ/DV) and differential voltage curves (DV, DV/DQ) of batteries with different electrolyte schemes and fresh battery under different current. (a) BASE-Elect; (b) FEMC-Elect; (c) DFEA-Elect.

Open Access Article. Published on 06 July 2023. Downloaded on 1/19/2026 4:26:41 PM.
This article is licensed under a Creative Commons Attribution-NonCommercial 3.0 Unported Licence.

process that occurred at around 4.1 V, it will cause the rapid contraction of the *c*-axis, which is considered to be the main reason for the particle crack.[34] In addition, the edge of the cracked particles will generate the transformation from the layered structure to the rock salt phase, which will reduce the migration channel of lithium ion. The rock salt phase of the ternary material is the insulation structure, which will significantly increase internal resistance of the battery. Moreover, the cracked particles also weaken the contact with the conductive agent, which can increase the internal resistance of the battery too. The cycled batteries' phase transformation peak that near 4.1 V of the electrolyte that adding the fluorinated solvent was divided into two peaks, and the difference of voltage is about 50 mV, which is usually considered to be the phase transformation peak of the single crystal and poly crystal of the ternary material. The appearance of single crystal phase transformation peak, indicating that the particles of cathode material have been obvious cracked. Since the poly crystal of the cathode material is the secondary spherical particles formed by the mall single crystals, the small single crystal particles split from secondary spherical particles showed the charging and discharge feature of the single crystal material. Thus, the phase transformation peak was divided into two peaks. There is no phase transformation peak separation in the BASE-Elect, indicating that the number of cracked particles is relatively low.

3.2 Surface and cross-section analysis

In order to verify the changes in battery activity materials, the fresh battery and cycled batteries were disassembled, and the FESEM analysis was performed on the activity material respectively. Fig. 6a shows the FESEM image of the cathode material of the fresh battery. It can be found that the cathode material is the large secondary spherical polycrystalline particles together with small polycrystalline particles. The particle structure is relatively complete. The surface morphology of cathode material that from the BASE-Elect has almost no change compared to the fresh battery, but some secondary spherical polycrystalline particles were cracked (Fig. 6b). The secondary spherical polycrystalline particles of the cathode material that from the fluorinated solvent scheme batteries showed a large area of particle crack (Fig. 6c and d), which is consistent with our previous analysis of DQ/DV. The particle crack degree of the FEMC-Elect was about 67%, while the DFEA-Elect was about 24%. As mentioned earlier, the cracked of the ternary material mainly occurs in the phase transformation process of H2 to H3 that at the voltage of 4.1 V. Due to the significant growth of polarization of the battery of the FEMC-Elect, which leads to the constant voltage charging time become longer. The increase in constant voltage charging time may exacerbate the phase transformation process of H2 to H3. Thus, its particle cracked ratio is relative higher. Fig. 6e–h show the cross-section FESEM images of different schemes. Compared with fresh battery, there is a clear gap between the active material and the Al foil of the cycled batteries, which may be related to the volume change of the electrode material in the charging and discharge process. The gap of the fluorinated solvent electrolyte schemes is even larger, which may be due to the removal of F^- from fluorinated solvent to form HF, which will cause the corrosion of Al foil. Thus, the gap becomes more obvious. Through the cross-section FESEM images of different schemes, it can be found that the particles of all schemes also were obviously cracked. The cracked secondary spherical polycrystalline particles will expose more active surfaces, and these newly exposed single crystal particles that

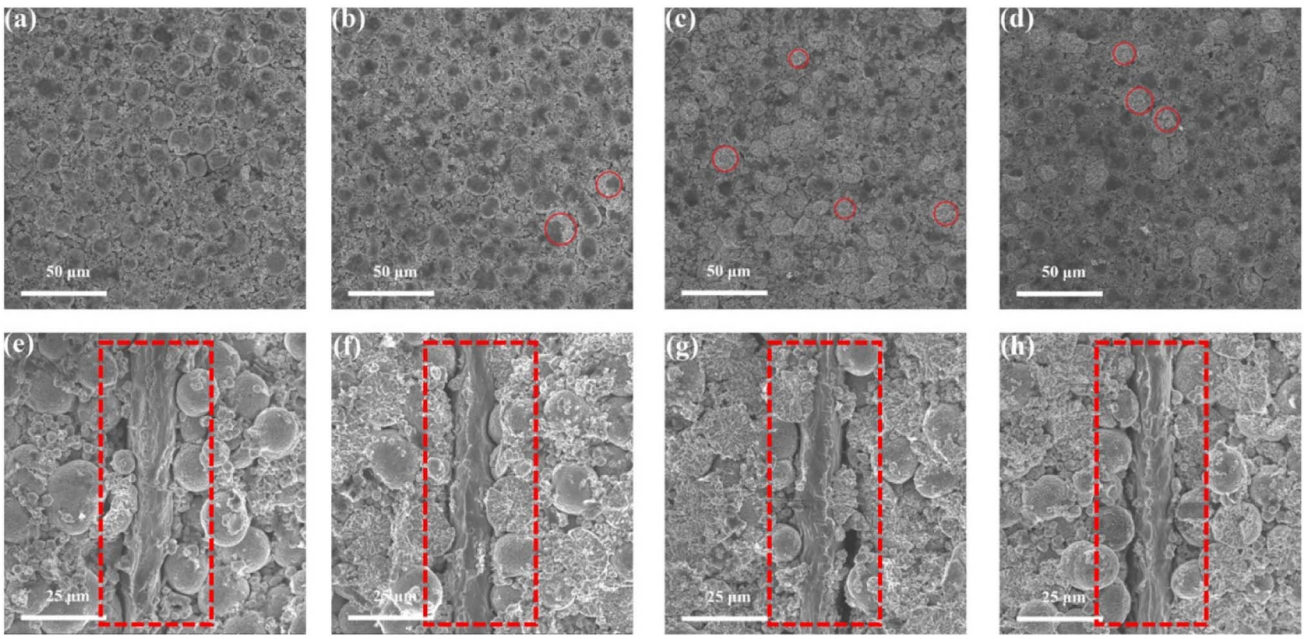

Fig. 6 The surface and cross-section FESEM images of cathode material of batteries with different electrolyte schemes and fresh battery under different current. (a) and (e) fresh; (b) and (f) BASE-Elect; (c) and (g) FEMC-Elect; (d) and (h) DFEA-Elect.

© 2023 The Author(s). Published by the Royal Society of Chemistry

Open Access Article. Published on 06 July 2023. Downloaded on 1/19/2026 4:26:41 PM.
This article is licensed under a Creative Commons Attribution-NonCommercial 3.0 Unported Licence.

make up the secondary spherical polycrystalline particles are relatively small and easy to be converted into insulating rock salt phase structure. In addition, the newly exposed surface does not directly contact with the conductive, which will also increase the internal resistance of battery. Moreover, more exposure of active sites will aggravate the contact between active materials and electrolyte, which will lead to the consumption of electrolyte and lead to more metal elements dissolution. The dissolved metal elements will catalyze side reactions of electrolyte, and further consume the active components of electrolyte.

In order to clarify the changes in particle size and volume after secondary ball particle crushing more clearly, particle size distribution statistics and BET detection were used respectively. Fig. 7a shows the particle size distribution of BASE-Elect scheme, which is mainly composed of large secondary spherical particles, with the D_{50} of approximately 12 μm. Some small particles also come from the size design of the cathode material itself. As shown in Fig. 7b, the particle size distribution of FEMC-Elect scheme was changed obviously, the proportion of small particles has significantly increased, indicating that a large number of secondary spherical particles have crashed and formed smaller particles, which is consistent with previous analysis. The same change also occurred on the cathode material of DFEA-Elect scheme, however, the proportion of small particles is relatively small, indicating that the degree of particle crash is lower than FEMC-Elect. Fig. 7d–f show the BET of different electrolyte schemes, the change in specific surface area is consistent with the change in particle size. As the increase of small particles caused by the crash of large particles, the specific surface area of the cathode material continues to increase.

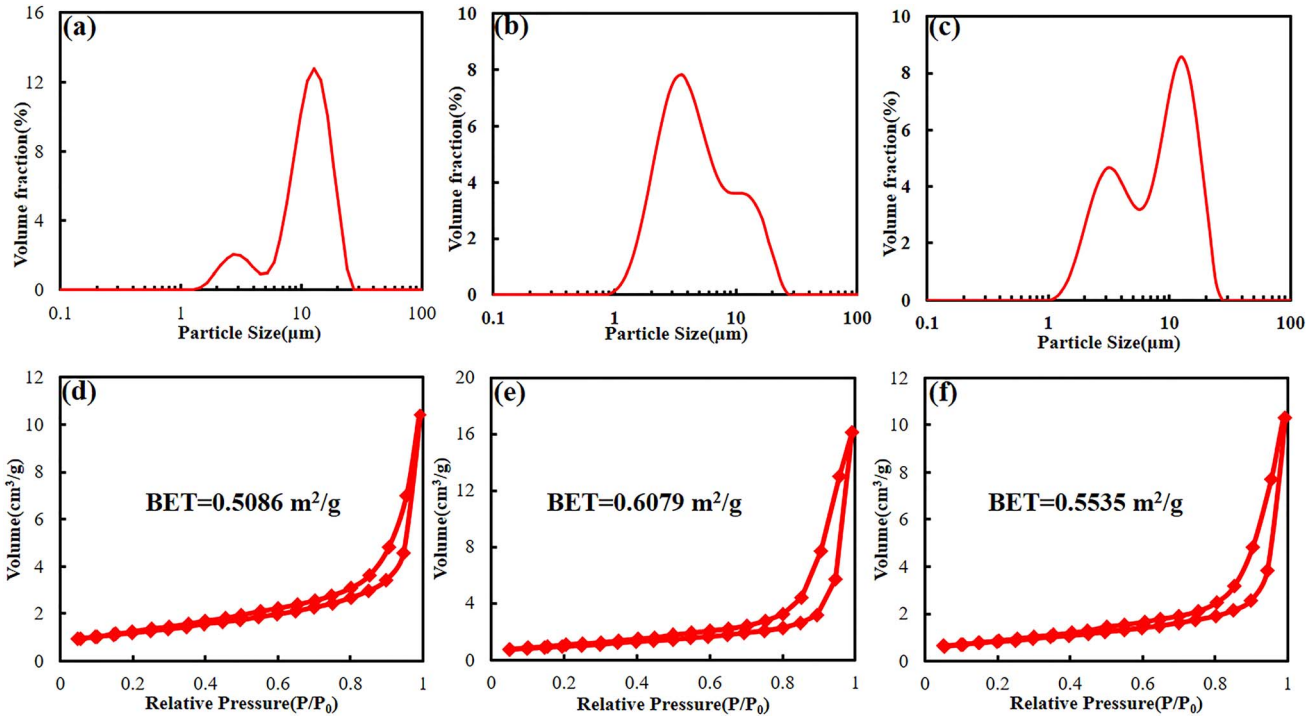

Fig. 7 The particle size distribution (a–c) and BET (d–f) of cathode material of batteries with different electrolyte schemes. (a and d) BASE-Elect; (b and e) FEMC-Elect; (c and f) DFEA-Elect.

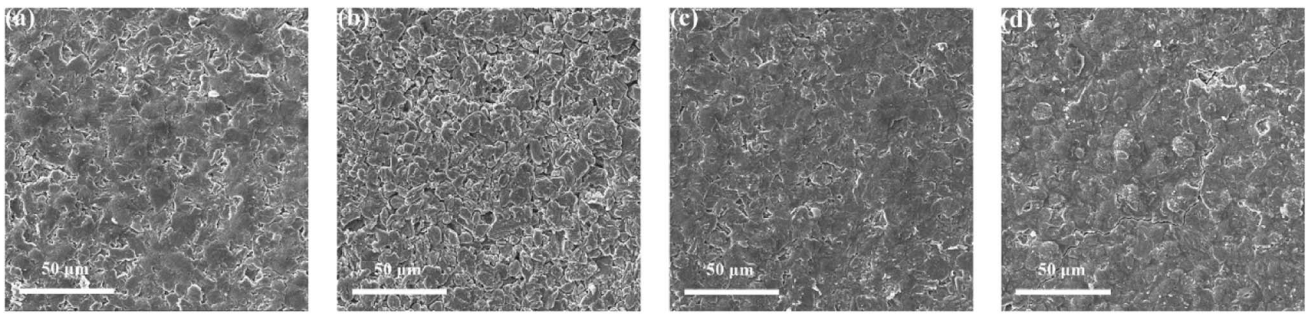

Fig. 8 The FESEM images of anode material of batteries with different electrolyte schemes and fresh battery under different current. (a) Fresh; (b) BASE-Elect; (c) FEMC-Elect; (d) DFEA-Elect.

Open Access Article. Published on 06 July 2023. Downloaded on 1/19/2026 4:26:41 PM. This article is licensed under a Creative Commons Attribution-NonCommercial 3.0 Unported Licence.

Table 2 ICP element content analysis of anode material for the different electrolyte schemes of recycled battery

	BASE-Elect	FEMC-Elect	DFEA-Elect
Element	ppm	ppm	ppm
Ni	1553.231	279.396	294.602
Co	178.663	28.305	30.092
Al	35.573	50.817	49.927
Li	22 602.03	38 539.98	25 367.08
Si	10 223.673	10 270.475	10 106.361

Fig. 8 shows the FESEM images of anode material of the fresh battery and cycled batteries. It can be seen from the figure that the SEI film with fluorinated solvent electrolyte schemes is relatively complete and dense, and the differences between the two schemes is negligible, while the SEI film of the BASE-Elect is severely cracked and relatively poor in integrity, which indicates that the addition of fluorinated solvent is more conducive to the formation of SEI film. In order to determine the metal dissolution and the lithium evolution, the anode material was tested by ICP. As shown in Table 2, the content of Ni and Co in the anode material of fluorinated solvent electrolyte schemes were significantly lower than that of the BASE-Elect, but the content of Al and Li shows the opposite trend. The low content of Ni and Co indicates that the metal dissolution of the cathode material is relative low, which may be attributed to the promotion of film formation by fluorinated solvents. Fluorinated solvents can not only promote the formation of SEI on the surface of anode material, but also facilitate the formation of CEI film on the surface of cathode material, thus, reducing the corrosion of electrolyte on the cathode material and reducing the dissolution of metal elements. The increase of Li may be due to the low conductivity of the electrolyte, which leads to the higher over potential of the anode during the charging and discharging process, making it easy to lead to the deposition of lithium ions in the anode material surface to form lithium. Therefore, the content of Li in the anode material with fluorinated solvent is relatively high. In order to determine the source of Al, the cathode material was tested by EDS. As shown in Table 3, the content of Al in the cathode material of the three electrolyte schemes is almost the same, which indicates that Al in the anode is not from the dissolution of the cathode material, but mainly come from the contribution of Al foil as the fluid collector, which is consistent with our previous analysis of the fluorinated solvent corrosion Al foil.

Table 3 EDS element content analysis of cathode material for the different electrolyte schemes of recycled battery

	BASE-Elect	FEMC-Elect	DFEA-Elect
Element	At/%	At/%	At/%
C	38.40	36.39	38.94
O	36.05	37.84	36.08
F	8.08	6.74	6.17
Al	0.40	0.41	0.39
P	0.19	0.15	0.13
S	0.11	0.16	0.12
Co	1.77	2.01	2.02
Ni	15.00	16.30	16.15
Sum	100.00	100.00	100.00

3.3 Crystal structure analysis

In order to characterize the change of lithium–nickel mixed arrangement of cathode materials, the XRD measurements were carried out on cathode materials of all schemes. As shown in Fig. 9, the cathode materials of all schemes showed complete ternary layered $LiNiO_2$ structure. However, the strength ratio of (003) and (104) is not the same. The ratio of the FEMC-Elect is the smallest, which indicates that the degree of lithium–nickel mixed arrangement is the highest. While the BASE-Elect showed the opposite result. The cell parameters and the degree of lithium–nickel mixed arrangement can be further obtained by XRD refinement. As shown in Table 4, the *a*-axis shrinkage and *c*-axis elongation of the FEMC-Elect are the most obvious, and the value of *c*/*a* is also the largest, which causes the small angle diffraction peak of XRD to shift to a small angle, while the large angle diffraction peak to shift to a large angle. The degree of lithium–nickel mixed arrangement has also become higher. In addition, because the lattice parameters of the cathode material in the FEMC-Elect change the most, this will lead to the highest degree of lattice fragmentation, which is consistent with the scanning results.

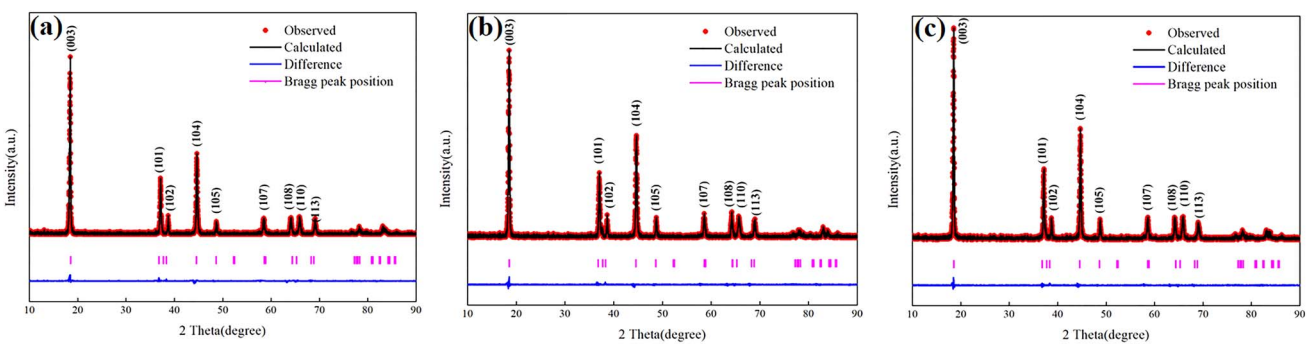

Fig. 9 The XRD patterns of cathode material of batteries with different electrolyte schemes and fresh battery under different current. (a) BASE-Elect; (b) FEMC-Elect; (c) DFEA-Elect.

© 2023 The Author(s). Published by the Royal Society of Chemistry

Open Access Article. Published on 06 July 2023. Downloaded on 1/19/2026 4:26:41 PM.
This article is licensed under a Creative Commons Attribution-NonCommercial 3.0 Unported Licence.

Table 4 Evolution of crystal structural parameters of the NCA cathode from neutron powder diffraction patterns for the different electrolyte schemes of recycled battery

Scheme	I_{003}/I_{104}	Lattice parameter/Å				Lithium–nickel mixed arrangement/%
		a	b	c	c/a	
BASE-Elect	2.217	2.834725	2.834725	14.421857	5.088	1.68
FEMC-Elect	1.767	2.743884	2.743884	14.364673	5.235	3.65
DFEA-Elect	1.923	2.808286	2.808286	14.391373	5.125	2.57

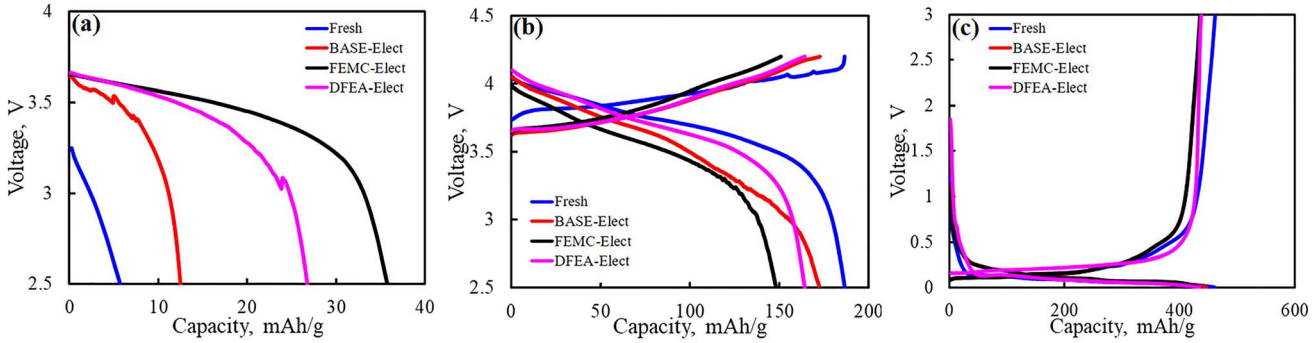

Fig. 10 (a) The first discharge curves of the cathode material; (b) the charge and discharge curves of cathode material; (c) the charge and discharge curves of anode material.

In order to clarify the contribution of cathode material and anode material to the capacity attenuation, it is necessary to assemble the coin cells with cathode material and anode material separately to evaluate the proportion of the individual capacity loss. Fig. 10a shows the first discharge capacity of the cathode material. For the cathode material after cycling, its first discharge capacity is usually caused by the lithium vacancy in the material, which is mainly caused by the loss of active lithium. Therefore, when the counter electrode is Li, it can be supplemented by the discharge process, which is expressed as the discharge capacity. This part of the capacity is not considered to be caused by the damage of the cathode structure. As shown in this figure, the FEMC-Elect exhibited the highest discharge capacity, which indicates that its active lithium loss is higher. The BASE-Elect shows the opposite result. Combined with the ICP results of the anode material, it is believed that the active lithium lost in this part is mainly contributed to the anode (including "dead lithium", SEI film and lithium precipitation). For fresh battery, the capacity loss may be attributed to the formation of SEI film. Fig. 10b shows the curve of subsequent charging and discharging, this part of the capacity is the residual capacity of the cathode material. And the capacity difference between cycled batteries and fresh battery is considered to be the irreversible capacity loss caused by the structural damage of the cathode material. It can be seen from the figure that the irreversible capacity loss of the FEMC-Elect is the largest, which may be related to its particle crack. A large number of particle crack leads to the destruction of the structural integrity of the cathode material, thus, the capacity decreased significantly. Due to the low number of particle crack, the irreversible capacity loss of the BASE-Elect is relatively low. Therefore, its capacity loss mainly comes from the loss of active lithium. Fig. 10c shows the test results of the coin cells of the anode material. It can be seen from the figure that the difference of the anode material capacity loss of the three electrolyte schemes is almost negligible, which indicates that the difference in battery cycle performance is mainly caused by the structural damage of the cathode material. The cracking of the secondary spherical particles of the cathode material will bring more active surfaces. These newly formed surfaces will form an insulating rock salt phase structure of ternary material, and the contact with the conductive agent will also become weak, which may lead to the consumption of electrolyte and increase the internal resistance of the battery. Therefore, the cycle performance of the battery reduced.

4 Conclusion

Integrate all analysis results, on the one hand, the introduction of fluorinated solvents will reduce the conductivity of the electrolyte, which will lead to an increase in the polarization of the battery. The increase in polarization will make the time of constant voltage charging of the battery longer during whole cycles. For ternary materials, the H2 to H3 phase transformation process at high voltage is the main reason of material crack. The increase in constant voltage charging time will intensify the phase transformation process, leading to a higher degree of material crack. The cracked particles will expose more active surfaces, and the newly formed active surface will form an insulating rock salt phase structure, and the contact with the conductive agent will also become weak, which will lead to an increase in the internal resistance of the battery and further

Open Access Article. Published on 06 July 2023. Downloaded on 1/19/2026 4:26:41 PM. This article is licensed under a Creative Commons Attribution-NonCommercial 3.0 Unported Licence.

increase the polarization of the battery; on the other hand, the addition of fluorinated solvent can promote the formation of the SEI film on anode and the CEI film on cathode, which has a protective effect on the dissolution of metal elements in the cathode material. Since the fast-charging cycle will not reach constant voltage charging, and the high temperature rise brought by fast-charging can inhibit the effect of electrolytic conductivity, so that the protective effect of fluorinated solvent on the cathode is dominant. Thus, improving the fast-charging performance of the battery. Therefore, fluorinated solvents have certain effects on improving the fast-charging performance of the battery, but may reduce the conventional cycle.

Conflicts of interest

The authors declare that they have no known competing financial interests.

Acknowledgements

There is no fund support for this work.

References

1 L. Wen, P. Oh, X. Liu, M.-J. Lee, W. Cho, S. Chae, Y. Kim and J. Cho, Nickel-Rich Layered Lithium Transitional-Metal Oxide for High-Energy Lithium-Ion Batteries, *Angew. Chem., Int. Ed.*, 2015, **54**, 4440–4458.

2 Gi Y. Kim, S. R. Park and J. Su Yu, Design and characteristics of low-resistance lithium-ion battery pack and its fast charging method for smart phones, *Int. J. Energy Res.*, 2021, 1–16.

3 A. Marongiu, M. Roscher and D. U. Sauer, Influence of the vehicle-to-grid strategy on the aging behavior of lithium battery electric vehicles, *Appl. Energy*, 2015, **137**, 899–912.

4 D. Bresser, K. Hosoi, D. Howell, L. Hong, Z. Herbert, K. Amine and S. Passerini, Perspectives of automotive battery R&D in China, Germany, Japan, and the USA, *J. Power Sources*, 2018, **382**, 176–178.

5 F. Sun, R. Xiong and H. He, A systematic state-of-charge estimation framework for multi-cell battery pack in electric vehicles using bias correction technique, *Appl. Energy*, 2016, **162**, 1399–1409.

6 T.-H. Kim, J.-S. Park, S. K. Chang, S. Choi, J. H. Ryu and H.-K. Song, The Current Move of Lithium Ion Batteries Towards the Next Phase, *Adv. Energy Mater.*, 2012, **2**, 860–872.

7 S. Yin, W. Deng, J. Chen, X. Gao, G. Zou, H. Hou and X. Ji, Fundamental and solutions of microcrack in Ni-rich layered oxide cathode materials of lithium-ion batteries, *Nano Energy*, 2021, **83**, 105854.

8 K. Jalkanen, J. Karppinen, L. Skogström, T. Laurila, M. Nisula and K. Vuorilehto, Cycle aging of commercial NMC/graphite pouch cells at different temperatures, *Appl. Energy*, 2015, **154**, 160–172.

9 R. Xiong, L. Li and J. Tian, Towards a smarter battery management system: A critical review on battery state of health monitoring methods, *J. Power Sources*, 2018, **405**, 18–29.

10 J. de Hoog, J.-M. Timmermans, D. Ioan-Stroe, M. Swierczynski, J. Jaguemont, S. Goutam, N. Omar, J. Van Mierlo and P. Van Den Bossche, Combined cycling and calendar capacity fade modeling of a Nickel-Manganese-Cobalt Oxide Cell with real-life profile validation, *Appl. Energy*, 2017, **200**, 47–61.

11 B. Stiaszny, J. C. Ziegler, E. E. Krauß, J. P. Schmidt and E. Ivers-Tiffée, Electrochemical characterization and post-mortem analysis of aged $LiMn_2O_4$-$Li(Ni_{0.5}Mn_{0.3}Co_{0.2})O_2$/graphite lithium ion batteries. Part I: Cycle aging, *J. Power Sources*, 2014, **251**, 439–450.

12 L. Su, J. Zhang, C. Wang, Y. Zhang, Z. Li, Y. Song, T. Jin and M. Zhao, Identifying main factors of capacity fading in lithium ion cells using orthogonal design of experiments, *Appl. Energy*, 2016, **163**, 201–210.

13 K. A. Severson, P. M. Attia, N. Jin, N. Perkins, B. Jiang, Z. Yang, M. H. Chen, M. Aykol, P. K. Herring, D. Fraggedakis, M. Z. Bazant, S. J. Harris, W. C. Chueh and R. D. Braatz, Data-driven prediction of battery cycle life before capacity degradation, *Nat. Energy*, 2021, **4**(5), 383–391.

14 K.-J. Park, H.-G. Jung, L.-Y. Kuo, P. Kaghazchi, C. S. Yoon and Y.-K. Sun, Improved Cycling Stability of Li $[Ni_{0.90}Co_{0.05}Mn_{0.05}]O_2$ Through Microstructure Modification by Boron Doping for Li-Ion Batteries, *Adv. Energy Mater.*, 2018, 1801202.

15 U.-H. Kim, L.-Y. Kuo, P. Kaghazchi, C. S. Yoon and Y.-K. Sun, Quaternary Layered Ni-Rich NCMA Cathode for Lithium-Ion Batteries, *ACS Energy Lett.*, 2019, **4**(2), 576–582.

16 Y. Liu, E. Cui, A. L. Neal, X. Zhang, Z. Li, Y. Xiao, Z. Du, F. Gao, X. Fan and C. Hu, Reducing water use by alternate-furrow irrigation with livestock wastewater reduces antibiotic resistance gene abundance in the rhizosphere but not in the non-rhizosphere, *Sci. Total Environ.*, 2019, **648**, 12–24.

17 L. Zhao, J. C. Bennett, A. George and M. N. Obrovac, SiC-Free Carbon–Silicon Alloys Prepared by Delithiation as LithiumIon Battery Negative Electrodes, *Chem. Mater.*, 2019, **31**, 3883–3890.

18 L. Hu, K. Amine and Z. Zhang, Fluorinated electrolytes for 5-V Li-ion chemistry: Dramatic enhancement of $LiNi_{0.5}Mn_{1.5}O_4$/graphite cell performance by a lithium reservoir, *Electrochem. Commun.*, 2014, **44**, 34–37.

19 X. Zuo, C. Fan, J. Liu, X. Xiao, J. Wu and J. Nan, Lithium Tetrafluoroborate as an Electrolyte Additive to Improve the High Voltage Performance of Lithium-Ion Battery, *J. Electrochem. Soc.*, 2013, **160**(8), A1199–A1204.

20 A. Ali, S. A. Odom, H. Tavassol, M. V. Schulmerich, H. Wu, R. Bhargava, A. A. Gewirth, J. S. Moore and K. Amine, 3-Hexylthiophene as a Stabilizing Additive for High Voltage Cathodes in Lithium-Ion Batteries, *J. Electrochem. Soc.*, 2013, **160**(2), A268–A271.

21 C. Gao, Q. Wang, S. Luo, Z. Wang, Y. Zhang, Y. Liu, A. Hao and R. Guo, High performance potassium-ion battery

© 2023 The Author(s). Published by the Royal Society of Chemistry

Open Access Article. Published on 06 July 2023. Downloaded on 1/19/2026 4:26:41 PM.
This article is licensed under a Creative Commons Attribution-NonCommercial 3.0 Unported Licence.

anode based on biomorphic Ndoped carbon derived from walnut septum, *J. Power Sources*, 2019, **415**, 165–171.

22 X. Zeng, G.-L. Xu, Y. Li, X. Luo, F. Maglia, C. Bauer, S. F. Lux, O. Paschos, S.-J. Kim, P. Lamp, J. Lu, K. Amine and Z. Chen, Kinetic. Study of Parasitic Reactions in LithiumIon Batteries: A Case Study on $LiNi_{0.6}Mn_{0.2}Co_{0.2}O_2$, *ACS Appl. Mater. Interfaces*, 2016, **8**(5), 3446–3451.

23 W. Li, H. Yaghoobnejad Asl, Q. Xie and A. Manthiram, Collapse of $LiNi_{1-x-y}Co_xMn_yO_2$ Lattice at Deep Charge Irrespective of Nickel Content in Lithium-Ion Batteries, *J. Am. Chem. Soc.*, 2019, **141**, 5097–5101.

24 Y.-K. Sun, S.-T. Myung, B.-C. Park, J. Prakash, I. Belharouak and K. Amine, High-energy cathode material for long-life and safe lithium batteries, *Nat. Mater.*, 2019, **8**, 320–324.

25 Y.-K. Sun, Z. Chen, H.-J. Noh, D.-J. Lee, H.-G. Jung, Y. Ren, S. Wang, C. S. Yoon, S.-T. Myung and K. Amine, Nanostructured high-energy cathode materials for advanced lithium batteries, *Nat. Mater.*, 2012, **11**, 942–947.

26 Y. Makimura, S. Zheng, Y. Ikuhara and Y. Ukyo, Microstructural Observation of $LiNi_{0.8}Co_{0.15}Al_{0.05}O_2$ after Charge and Discharge by Scanning Transmission Electron Microscopy, *J. Electrochem. Soc.*, 2012, **159**(7), A1070–A1073.

27 S. Watanabe, M. Kinoshita, T. Hosokawa, K. Morigaki and K. Nakura, Capacity fade of $LiAl_yNi_{1-x-y}Co_xO_2$ cathode for lithium-ion batteries during accelerated calendar and cycle life tests (surface analysis of $LiAl_yNi_{1-x-y}Co_xO_2$ cathode after cycle tests in restricted depth of discharge ranges), *J. Power Sources*, 2014, **258**, 210–217.

28 K.-J. Park, M.-J. Choi, F. Maglia, S.-J. Kim, K.-H. Kim, C. S. Yoon and Y. K. Sun, High-Capacity Concentration Gradient $Li[Ni_{0.865}Co_{0.120}Al_{0.015}]O_2$ Cathode for Lithium-Ion Batteries, *Adv. Energy Mater.*, 2018, 1703612.

29 C. R. Jarvis, M. J. Lain, M. V. Yakovleva and Y. Gao, A prelithiated carbon anode for lithium-ion battery applications, *J. Power Sources*, 2006, **162**, 800–802.

30 M. He, C.-C. Su, Z. Feng, L. Zeng, T. Wu, M. J. Bedzyk, F. Paul, Y. Wang and Z. Zhang, High Voltage $LiNi_{0.5}Mn_{0.3}Co_{0.2}O_2$/Graphite Cell Cycled at 4.6 V with a FEC/HFDEC-Based Electrolyte, *Adv. Energy Mater.*, 2017, 1700109.

31 Y.-M. Lee, K.-M. Nam, E.-H. Hwang, Y.-G. Kwon, D.-H. Kang, S.-S. Kim and S.-W. Song, Interfacial Origin of Performance Improvement and Fade for 4.6 V $LiNi_{0.5}Co_{0.2}Mn_{0.3}O_2$ Battery Cathodes, *J. Phys. Chem. C*, 2014, **118**, 10631–10639.

32 J. Xia, R. Petibon, A. Xiao, W. M. Lamanna and J. R. Dahn, The effectiveness of electrolyte additives in fluorinated electrolytes for high voltage $Li[Ni0_{.4}Mn_{0.4}Co_{0.2}]O_2$/graphite pouch Li-ion cells, *J. Power Sources*, 2016, **330**, 175–185.

33 C. Wang, L. Tan, H. Yi, Z. Zhao, X. Yi, Y. Zhou, J. Zheng, J. Wang and L. Li, Unveiling the impact of residual Li conversion and cation ordering on electrochemical performance of Co-free Ni-rich cathodes, *Nano Res.*, 2022, **15**(10), 9038–9046.

34 H. H. Sun and A. Manthiram, Impact of microcrack generation and surface degradation on a nickel-rich layered $Li[Ni_{0.9}Co_{0.\ 05}Mn_{0.05}]O_2$ cathode for lithium-ion batteries, *Chem. Mater.*, 2017, **29**, 8486–8493.